CYBERNETICS AND PHYSICS, VOL. 13, NO. 1, 2024, 77–81

SPATIAL GUIDANCE AND CONTROL OF A SPACE ROBOT DURING FLIGHTS IN A LOW-ORBIT CONSTELLATION OF EARTH OBSERVATION MINI-SATELLITES

Yevgeny Somov[1,2]
[1] Dynamics and Motion Control
Samara Federal Research
Scientific Center RAS
[2]Navigation, Guidance and Control
Samara State Technical University
Samara, Russia
e_somov@mail.ru

Sergey Butyrin[1,2]
[1] Dynamics and Motion Control
Samara Federal Research
Scientific Center RAS
[2]Navigation, Guidance and Control
Samara State Technical University
Samara, Russia
butyrinsa@mail.ru

Sergey Somov[1,2]
[1] Dynamics and Motion Control
Samara Federal Research
Scientific Center RAS
[2]Navigation, Guidance and Control
Samara State Technical University
Samara, Russia
s_somov@mail.ru

Article history:
Received 08.12.2023, Accepted 09.06.2024

Abstract

Algorithms for guidance and control of a space robot-manipulator when approaching mini-satellites in adjacent orbital planes of the earth-survey constellation and the results of their computer verification are presented. The article examines the issues on astrodynamics of a space robot in the gravitational fields of the Earth, Moon and Sun, taking into account the aerodynamic resistance to its movement in low orbit. At the same time, an electro-reactive propulsion unit and a cluster of gyroscopic drives are used to create vectors of control forces and torques. The most important are new methods and results for the space robot digital control during its flight between mini-satellites.

Key words

Space robot, constellation of mini earth observation satellites, flights and rendezvous, guidance and control.

Abbreviations

AN = Ascending Node
AOCS = Attitude and Orbit Control System
BRF = Body Reference Frame
EPU = Electric Propulsion Unit
GD = Gyrodine
GMC = Gyroscopic Moment Cluster
IRF = Inertial Reference Frame
MRP = Modified Rodrigues Parameters
ORF = Orbital Reference Frame
SINS = Strapdown Inertial Navigation System
SRM = Space Robot-Manipulator
STC = Star Tracker Cluster

1 Introduction

The main trend in modern space systems for remote sensing of the Earth is the transition to constellations of optoelectronic (SkySat) and radar (Capella-36) mini-satellites with a high frequency of earth survey from low orbits [Crisp et al., 2021; Rodriguez-Donaire et al., 2020; Lappas and Kostopoulos, 2020; Somov et al., 2021b; Somov et al., 2023b]. With a service life of up to 5 years, such satellites have a mass of up to 500 kg and large-sized solar array panels to power onboard equipment, including an attitude and orbit control system (AOCS) with electric propulsion units (EPUs) and a gyro moment cluster (GMC) based on gyrodines (GDs). Measuring the coordinates of the spacecraft (SC) motion is carried out by a strapdown inertial navigation system (SINS) with correction based on signals from navigation satellites and a star tracker cluster (STC). In-flight refueling of EPU is not economically viable for "cheap" micro-satellites weighing up to 100 kg, but for mini-satellites equipped with "expensive" onboard equipment (telescope, SINS, STC, GMC, EPU, etc.), it is necessary to study the extension of a service life up to 20 years by the EPU refueling while using space robot-manipulators (SRMs). For an orbital constellation of Earth observation mini-satellites in low sun-synchronous orbits, three SC in the vicinity of each base orbital plane [Somov et al., 2023b], the problems of the SRM motion control are very relevant when approaching mini-satellites.

The article discusses the problems of performing such maneuvers of the SRM near one base orbital plane while estimating the time duration and fuel consumption of the EPU during the SRM flights between mini-satellites.

2 Models and the problem statement

We use the following reference frames (RF): inertial (IRF $\mathrm{O}_{\oplus}\mathrm{X}^{\mathrm{i}}\mathrm{Y}^{\mathrm{i}}\mathrm{Z}^{\mathrm{i}}$, basis $\mathbf{I}_{\oplus}$ with unit vectors $\mathbf{i}_i, i = 1,2,3 \equiv 1 \div 3$), orbital (ORF $Ox^{\circ}y^{\circ}z^{\circ}$, basis $\mathbf{O}$ with unit vectors of radial $\mathbf{r}^{\circ}$, transversal $\boldsymbol{\tau}^{\circ}$, binormal $\mathbf{n}^{\circ}$) and associated with the SRM body (BRF $Oxyz$, basis $\mathbf{B}$) reference frames with the origin at its mass center O. We assume that the thrust vector $\mathbf{P}^{\mathrm{e}}$ of the plasma EPU is directed along the BRF axis Oy. In the IRF $\mathbf{I} \equiv \mathbf{I}_{\oplus}$, the BRF orientation is defined by quaternion $\boldsymbol{\Lambda}_{\mathrm{I}}^{b} \equiv \boldsymbol{\Lambda} = (\lambda_0, \boldsymbol{\lambda})$, $\boldsymbol{\lambda} = \{\lambda_i\}$ and with respect to ORF – by column $\boldsymbol{\phi}=\{\phi_i\}$ of Euler-Krylov angles ϕ_1 (yaw), ϕ_2 (roll) and ϕ_3 (pitch). We use notation $\boldsymbol{\omega}(t)$ and $\boldsymbol{\varepsilon}(t)$, $\mathbf{r}(t)$ and $\mathbf{v}(t)$ for vectors of the SC body angular velocity and acceleration, its mass center's position and progressive velocity in the IRF as well as symbols $\langle\cdot,\cdot\rangle$, $\{\cdot\} = \mathrm{col}(\cdot)$, $[\cdot] = \mathrm{line}(\cdot)$ for vectors and $[\times], (\cdot)^{\mathrm{t}}$ for matrices. We apply vector of the modified Rodrigues parameters (MRP) $\boldsymbol{\sigma}=\{\sigma_i\}=\mathbf{e}\tan(\Phi/4)$ with Euler unit vector $\mathbf{e}$ and angle Φ. Vector $\boldsymbol{\sigma}$ is one-one connected with quaternion $\boldsymbol{\Lambda}$ by explicit relations. Collinear GD pair is named as *Scissored Pair Ensemble* (*SPE*) [Crenshaw, 1973]. Column $\boldsymbol{\mathcal{H}}(\boldsymbol{\beta}) \equiv \mathrm{h}_g\mathbf{h}(\boldsymbol{\beta}) = \mathrm{h}_g\Sigma\mathbf{h}_p(\beta_p)$ with the columns $\boldsymbol{\beta} \equiv \{\beta_p\}$, $p = 1 \div 4$ and $\mathbf{h}(\boldsymbol{\beta}) \in \boldsymbol{\mathcal{S}} \subset \mathbb{R}^3$, presents the angular momentum (AM) vector of the GMC by scheme *2-SPE* (Fig. 1) [Somov et al., 2021a; Somov et al., 2023a; Somov et al., 2023b], where h_g is own AM of each GD. With $|\mathbf{h}_p| = 1\ \forall p = 1 \div 4$, in the park state this scheme has the normed AM vector $\mathbf{h}(\boldsymbol{\beta}) = \mathbf{0}$.

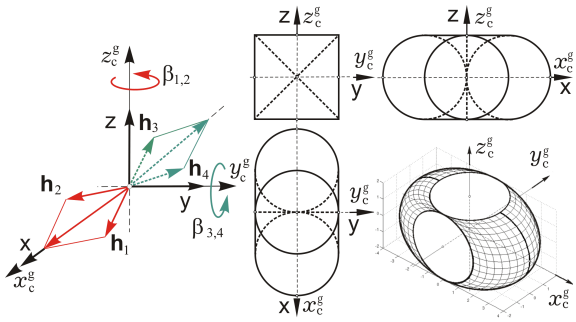

Figure 1. The GMC scheme *2-SPE* based on four GDs

The SRM body is considered as a solid with mass m and inertia tensor $\mathbf{J}$, model of its motion has the form

$$\begin{aligned} &\mathbf{r}' + \boldsymbol{\omega} \times \mathbf{r} = \mathbf{v};\ m(\mathbf{v}' + \boldsymbol{\omega} \times \mathbf{v}) = \mathbf{P}^{\mathrm{e}} + \mathbf{F}^{\mathrm{d}};\\ &\dot{\boldsymbol{\Lambda}} = \boldsymbol{\Lambda} \circ \boldsymbol{\omega}/2; \quad \mathbf{J}\dot{\boldsymbol{\omega}} + \boldsymbol{\omega} \times \mathbf{G} = \mathbf{M}^{\mathrm{g}} + \mathbf{M}^{\mathrm{d}}. \end{aligned} \tag{1}$$

Here vector $\mathbf{G} = \mathbf{J}\boldsymbol{\omega} + \boldsymbol{\mathcal{H}}$ and $\mathbf{M}^{\mathrm{g}} = -\boldsymbol{\mathcal{H}}'$ represents the GMC control torque vector, $\mathbf{F}^{\mathrm{d}}$ and $\mathbf{M}^{\mathrm{d}}$ are the vectors of external disturbing forces and torques, and finally, $(\cdot)'$ is the symbol of local time derivative. With using *Jacobi* matrix $\mathbf{A}_{\mathrm{h}}(\boldsymbol{\beta}) = \partial\mathbf{h}(\boldsymbol{\beta})/\partial\boldsymbol{\beta}$, vector $\mathbf{M}^{\mathrm{g}}$ is represented by the following relations with digital control vector $\mathbf{u}_k^{\mathrm{g}}$: $\mathbf{M}^{\mathrm{g}} = -\boldsymbol{\mathcal{H}}' = -\mathrm{h}_g\mathbf{A}_{\mathrm{h}}(\boldsymbol{\beta})\mathbf{u}_k^{\mathrm{g}}(t); \dot{\boldsymbol{\beta}} = \mathbf{u}_k^{\mathrm{g}}(t) \equiv \{\mathrm{u}_{pk}^{\mathrm{g}}(t)\}$, where control $\mathrm{u}_{pk}^{\mathrm{g}}(t) = \mathrm{Zh}[\mathrm{sat}(\mathrm{qntr}(u_{pk}^{g}, u_g^{\mathrm{o}}), u_g^{\mathrm{m}}), T_u]$ is forming $\forall k \in \mathbb{N}_0 \equiv [0, 1, 2, \dots)$ with a period T_u.

For a given the SRM angular guidance law $\boldsymbol{\Lambda}^p(t)$, $\boldsymbol{\omega}^p(t)$, $\boldsymbol{\varepsilon}^p(t)$ the error quaternion $\boldsymbol{\mathcal{E}} = (e_0, \mathbf{e}) = \tilde{\boldsymbol{\Lambda}}^p \circ \boldsymbol{\Lambda}$ with the vector $\mathbf{e} = \{e_i\}$, corresponds to the attitude error matrix $\mathbf{C}^{\mathrm{e}} = \mathbf{I}_3 - 2[\mathbf{e}\times]\mathbf{Q}_{\mathrm{e}}^{\mathrm{t}}$ with $\mathbf{Q}_{\mathrm{e}} = \mathbf{I}_3 e_0 + [\mathbf{e}\times]$ and the angular error vector $\delta\boldsymbol{\phi} = \{\delta\phi_i\} = 2e_0\mathbf{e}$. The vector $\delta\boldsymbol{\phi}$ is discrete filtered and then values of mismatch vector $\boldsymbol{\epsilon}_k^{\mathrm{f}} = -\boldsymbol{\phi}_k^{\mathrm{f}}$ are applied in the GMC digital control law

$$\begin{aligned} &\mathbf{g}_{k+1} = \mathbf{B}\mathbf{g}_k + \mathbf{C}\boldsymbol{\epsilon}_k^{\mathrm{f}};\ \ \tilde{\mathbf{m}}_k = \mathbf{K}(\mathbf{g}_k + \mathbf{P}\boldsymbol{\epsilon}_k^{\mathrm{f}});\\ &\mathbf{M}_k^{\mathrm{g}} = \boldsymbol{\omega}_k \times \mathbf{G}_k + \mathbf{J}(\mathbf{C}_k^{\mathrm{e}}\boldsymbol{\varepsilon}_k^{p} + [\mathbf{C}_k^{\mathrm{e}}\boldsymbol{\omega}_k^{p}\times]\boldsymbol{\omega}_k + \tilde{\mathbf{m}}_k), \end{aligned} \tag{2}$$

where for $d_u \equiv 2/T_u$, $a_i \equiv (d_u\tau_{1i} - 1)/(d_u\tau_{1i} + 1)$ elements of diagonal matrices $\mathbf{K}$, $\mathbf{B}$, $\mathbf{P}$ and $\mathbf{C}$ are computed as $b_i \equiv (d_u\tau_{2i} - 1)/(d_u\tau_{2i} + 1)$; $p_i \equiv (1 - b_i)/(1 - a_i)$; $c_i \equiv p_i(b_i - a_i)$ with adaptive-robust tuning the parameters τ_{1i}, τ_{2i} and k_i. Next, the GMC control torque vector $\mathbf{M}_k^{\mathrm{g}}$ (2) is "re-calculated" into vector $\mathbf{u}_k^{\mathrm{g}}$ of the GD digital commands using explicit function for the AM distribution between GDs [Matrosov and Somov, 2004].

In the column $\mathbf{q}_{\mathrm{r}} = \{\Omega, i, \omega_\pi, p, e, u\}$ of osculating coordinates for the position vector $\mathbf{r}$ of the SC in orbit, we traditionally distinguish (i) three elements of the orbit orientation – the longitude Ω of ascending node (AN), inclination i, argument of orbit perigee ω_π, and (ii) three elements that determine the size, shape of the orbit as well as the SC position in orbit – focal parameter p, eccentricity e and argument of orbital latitude $u(t)$, which sometimes is named as "orbital latitude" and is related with the true anomaly $\nu(t)$ by the ratio $u(t) = \omega_\pi + \nu(t)$.

When the SRM approaches mini-satellites (targets) to refuel their EPU, the SRM maneuvers consist of flights between the SC orbits. Each flight consists of three stages: (i) rotation of the SRM's orbital plane until it is aligned with orbital plane of the target, (ii) phasing the SRM's position with that target in coplanar orbits, and (iii) final rendezvous of the SRM with the target.

The problem is to develop the SRM guidance and control laws while obtaining the estimates of the duration and EPU fuel consumption during robot flights between mini-satellites. To solve it, we use methods of controlled space flight mechanics [Elyasberg, 1965; Battin, 1999; Alfriend et al., 2010; Vallado, 2013; Baranov, 2016; Curtis, 2020], including model of the SC movements and rendezvous in a gravitational field [Clohessy and Wiltshire, 1960] and its further developments directly taking into account the second harmonic of the gravitational geopotential [Schweighart and Sedwick, 2002], [Alfriend and Yan, 2005; Sullivan et al., 2017].

3 The SRM control when changing orbital plane

In the theory of instantaneous velocity impulses of the SC translational motion, the solution to the problem of the orbital plane turn [Curtis, 2020] is based on changing the direction of the transversal component of the SRM velocity vector $\mathbf{v}_1$ in the plane of the first orbit (Fig. 2, blue) by an angle $\Delta\Omega$ to obtain the velocity vector $\mathbf{v}_2$ in the plane of the second orbit, Fig. 2, green. When the SRM is located on the line of intersection

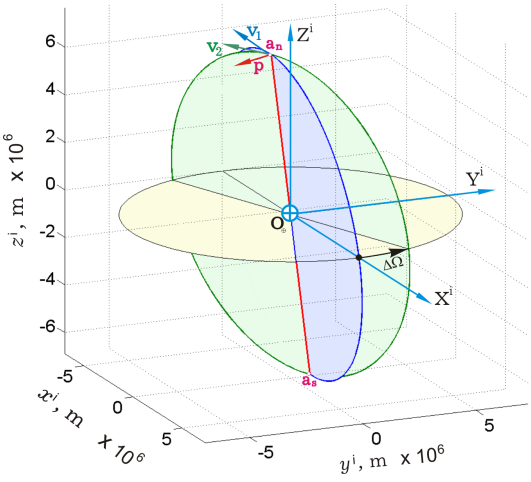

Figure 2. Scheme of changing the longitude of the orbit AN

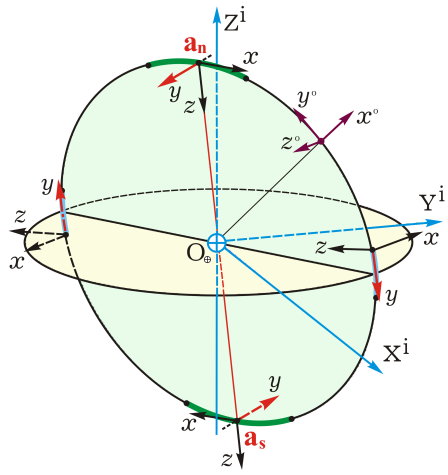

Figure 3. Scheme of the SRM control when inter-orbital flights

of these orbits at one of the apexes – see the points $\mathbf{a_n}$ or $\mathbf{a_s}$ most distant from the earth's equator in the northern or southern hemispheres of the celestial sphere (Fig. 3), the modulus of the required velocity impulse $\Delta \mathrm{v} = |\Delta \mathbf{v}| \equiv |\mathbf{v}_2 - \mathbf{v}_1|$ with $\mathrm{v}_1 = |\mathbf{v}_1|$ is calculated by the relation $\Delta \mathrm{v} = 2\mathrm{v}_1 \sin \Delta\Omega/2$. With low EPU thrust, the required velocity impulse cannot be realized in a short time interval, at which the SC orientation can be considered constant. Therefore, the important problem of determining the variable direction of the EPU thrust vector arises, at which the necessary maneuver of the SRM transition to a given orbital plane is implemented.

The velocity impulse vector $\Delta\mathbf{v}$ belongs to a plane tangent to both orbits and, therefore it is perpendicular to the line of intersection of these orbit planes. In the case $\Delta\Omega \to 0$, this condition is preserved, and position of the plane intersection line tends to the SRM position vector $\mathbf{r}$ with the unit vector $\mathbf{r}^\circ = \{r_1^\circ, r_2^\circ, r_3^\circ\}$ at the point of the corresponding apex. The change in the longitude of the SRM orbit's AN is representing by its turning around the Earth's rotation axis with the unit vector $\mathbf{i}_3 = \{0, 0, 1\}$.

All apexes of the SRM orbits are located on circles in planes parallel to the equatorial plane, and the unit vector $\mathbf{p}$ of the control acceleration along the axis Oy of the robot BRF is always directed from the IRF axis $\mathrm{O}_\oplus \mathrm{Z}^\mathrm{i}$ (Fig. 3) and belongs to the plane $\mathbf{Q}(\mathbf{r}^\circ, \mathbf{i}_3)$. Consequently, the unit vector $\mathbf{p}$ of the EPU thrust vector should be formed according to the relation $\mathbf{p} = \mathbf{b}/\mathrm{b}$, where vector $\mathbf{b} \equiv (\mathbf{i}_3 \times \mathbf{r}^\circ) \times \mathbf{r}^\circ$ and $\mathrm{b} = |\mathbf{b}|$. The result is the angular guidance law for the thrust vector $\mathbf{P}^\mathrm{e} = \mathrm{P}^\mathrm{m}\mathbf{p}\,\mathrm{sign}\, r_3^\circ$ of the plasma EPU, where parameter P^m represents the nominal value of the thrust.

With this guidance law, the efficiency of moving the AN longitude decreases when the SRM moves away from the corresponding apex. Therefore, there is rational to apply this law only near apexes, the passage of which occurs during the time intervals determined by the forecast of the SRM orbital movement. The forecast is performed at each turnover of the robot's orbit, based on analytical relations using measurements of the SRM position and velocity vectors. Here the time moments t_n and t_s of passage the northern and southern apexes are determined, as well as the time intervals for switching on the EPU $\forall t \in [t_j - T_d,\, t_j + T_d],\ j = \mathrm{n}, \mathrm{s}$ with the half value T_d of the full duration $S_d = 2T_d$ of switching on the EPU. Such intervals are displaying in Fig. 3 by sections of the SRM orbit, highlighted in green.

The SRM angular guidance is determined by the orientation matrix $\mathbf{A}_\mathrm{i}^\mathrm{b} = \{\mathbf{a}_i^\mathrm{t}\}$ at the columns $\mathbf{a}_1 = \mathbf{r}^\circ \times \mathbf{p}$, $\mathbf{a}_2 = \mathbf{p}$ and $\mathbf{a}_3 = \mathbf{a}_1 \times \mathbf{p}$, as well as by the quaternion $\mathbf{\Lambda}$ and MPR vector $\boldsymbol{\sigma}$. On each turnover of the orbit, in the vicinity of its ascending and descending nodes, two SRM turnings are performed at an angle of ≈ 180 deg (in Fig. 3 such parts are highlighted in blue) with the assignment of boundary conditions for the SRM transition through the apexes when the EPU is running.

4 The SRM control when phasing and rendezvous

Phasing is performed when two SC moving in close coplanar orbits approach each other due to a change in the average angular orbital velocity for one of them.

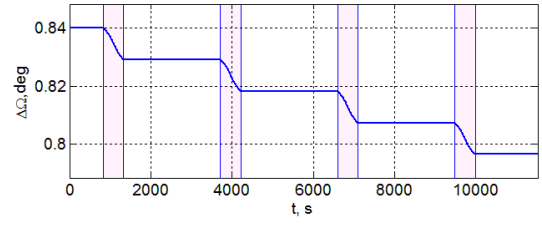

Figure 4. Difference in the AN longitude at the first two turnovers

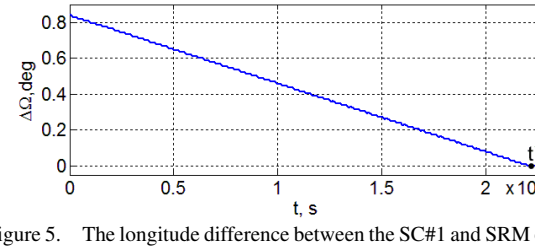

Figure 5. The longitude difference between the SC#1 and SRM orbits

In the theory of instantaneous velocity pulses, phasing is achieved through the formation of a velocity vector pulse at the perigee of the SRM orbit to change its average orbital velocity and, after one turnover of the phasing orbit, the formation of a reverse pulse $-\Delta\mathbf{v}$ to return the SRM to its original orbit [Curtis, 2020]. The pulses are formed in the corresponding directions of orbital transversal unit vector $\boldsymbol{\tau}^\circ$. The EPU low thrust is taken into account in calculating the parameters of the phasing trajectory with centering the time of the EPU turning on / off relative to the time t_π of perigee $\boldsymbol{\pi}$ passage. Solving the problem of approaching the SRM to the "aiming" point at a given distance from the serviced mini-satellite begins with synthesis of the SRM guidance law during translational motion. Here, the main parameters are the accelerating and braking instantaneous pulses of the SRM velocity, as well as the duration of the robot maneuver. Next, the Clohessy-Wiltshire equations and their modifications are used, taking into account the features of the distribution of the EPU required velocity pulses and onboard forecast of disturbances based on available measurements [Somov et al., 2023a].

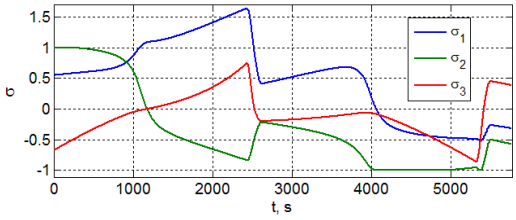

Figure 6. The MRP vector during the SRM turns at the first turnover

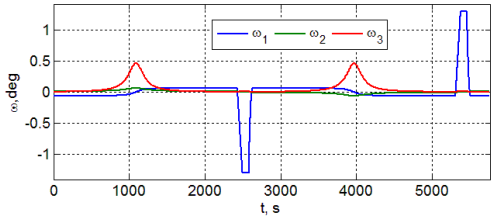

Figure 7. Angular velocity vector of SRM turns at the first turnover

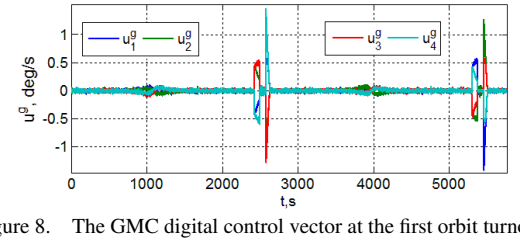

Figure 8. The GMC digital control vector at the first orbit turnover

5 Computer simulation results

A simulation was carried out for the SRM flights between adjacent orbits of mini-satellites in a constellation of three spacecraft in sun-synchronous orbits, spaced apart in the AN longitude by an angle $\Delta\Omega = 0.84$ deg.

The parameters of this constellation correspond to an areal survey of the Sea of Marmara and the environs of Istanbul, all details are presented in [Somov et al., 2023b]. Here we use models (1) and (2) for movement of the SRM with a mass m of 1500 kg and an inertia tensor $\mathbf{J} = \mathrm{diag}(1600, 1200, 1800)$ kg m s^2 taking into account gravitational disturbances from the Moon, Sun and second harmonic of the gravitational geopotential, the EPU with thrust $\mathrm{P}^{\mathrm{m}} = 6$ N at an exhaust velocity of the working fluid of 17363.7 m/s. Simulation of the SRM turning maneuvers was performed using the GMC with the own AM of each gyrodine $\mathrm{h}_g = 30$ Nms and digital control with the period $T_u = 0.25$ s.

Figure 4 shows changes in the difference in the AN longitude of the SRM orbit at the first two orbit turnover when the EPU is turned on in the vicinities of apexes, which are highlighted in pink. The change in the difference $\Delta\Omega(t)$ in the AN longitude of the SRM orbit is demonstrated in Fig. 5, where the flight between the orbits of SC#1 and SC#2 ends at the time moment t^*= 220200 s (the time duration $T_m = 2.55$ day) with a working fluid consumption of 13.26 kg.

Figures 6 and 7 show the program changes in the MRP $\boldsymbol{\sigma}$ vectors and angular velocity $\boldsymbol{\omega}$ when two SRM turns at the first orbit turnover, and vector of the GD digital commands at such SRM turns is presented in Fig. 8. The results of simulating the SRM phasing when its approaches SC#1 in the orbital plane are presented by the change of the difference in their orbital latitudes in Fig. 9. Disturbances, errors in forecast and the SRM orientation control when "distribution" of a required velocity pulse at a given time interval, taking into account the EPU low thrust, do not allow phasing to be performed with high accuracy. Therefore, additional stages of approaching

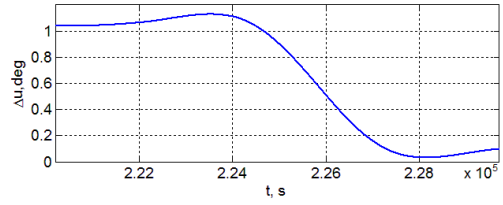

Figure 9. Difference in orbital latitude between SC#1 and SRM

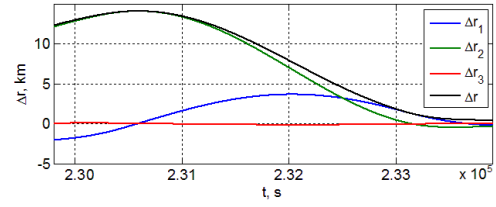

Figure 10. Vector of the SRM range at the first stage of approach

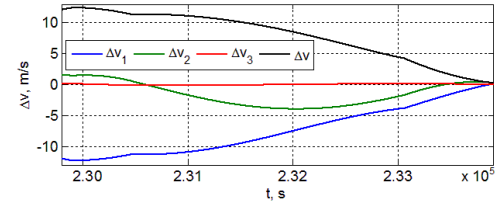

Figure 11. Vector of difference between velocities at the first stage

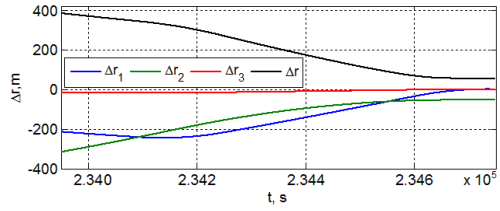

Figure 12. Vector of the SRM range at the second stage of approach

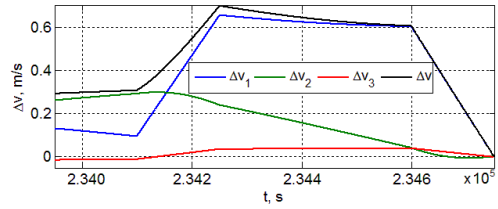

Figure 13. Vector of difference between velocities at the second stage

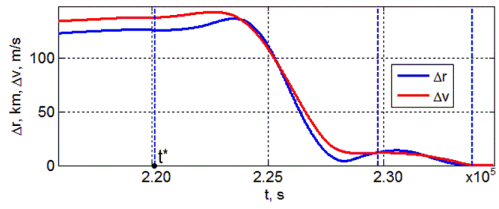

Figure 14. Modules of range vectors and velocity differences

the SRM with the target are necessary, presented in detail in Figs. 10 – 13, where the modules of vectors are marked in black. Figure 14 shows a general diagram of the change in the modules of the range vectors and the difference in velocities of the robot and targets, indicated at the final stages of the SRM maneuvering. Here, three blue dotted vertical lines separate: (i) orbital plane rotation and phasing (left line), (ii) phasing and the first stage of approach (middle line) and, finally, (iii) the rightmost line separates the first and second additional sequentially performed stages of rendezvous.

Conclusion

The developed algorithms for control of a space robot during its flights between mini-satellites in low orbits in a constellation of the Earth survey are described and results of computer simulation are presented. Estimates of the time duration and fuel consumption of the electric propulsion unit during robot flights were obtained. These results are useful for study and research in astrodynamics [Vallado, 2013] as a branch of astrophysics https://en.wikipedia.org/wiki/Astrophysics.

References

Alfriend, K., Vadali, S., Gurfil, P., et al. (2010). *Spacecraft Formation Flying: Dynamics, Control and Navigation*. Butterworth-Heinemann: Elsevier. 402 p.

Alfriend, K. and Yan, H. (2005). Evaluation and comparison of relative motion theories. *J. Guid. Control. Dyn.*, **28** (2), pp. 254–261.

Baranov, A. (2016). *Maneuvering Spacecraft in the Vicinity of a Circular Orbit*. Sputnik +, Moscow. 512 p.

Battin, R. (1999). *An Introduction to the Mathematics and Methods of Astrodynamics*. AIAA, Reston. 796 p.

Clohessy, W. and Wiltshire, R. (1960). Terminal guidance system for satellite rendezvous. *J. Astronaut. Sci.*, **27** (9), pp. 653–678.

Crenshaw, J. (1973). 2-SPEED, a single-gimbal moment gyro attitude control system. *AIAA Paper*, (73-895), pp. 1–10.

Crisp, N., Roberts, P., Romano, F., et al. (2021). System modelling of very low earth orbit satellites for earth observation. *Acta Astronaut.*, **187**, pp. 475–491.

Curtis, H. (2020). *Orbital Mechanics for Engineering Students*. Butterworth-Heinemann: Elsevier. 946 p.

Elyasberg, P. (1965). *Introduction to the Theory of Flight of Artificial Earth Satellites*. Nauka, Moscow. 540 p.

Lappas, V. and Kostopoulos, V. (2020). A survey on small satellite technologies and space missions for geodetic applications. In *Satellites Missions and Technologies for Geosciences*, chapter 8, pp. 1–22. IntechOpen.

Matrosov, V. and Somov, Y. (2004). Nonlinear problems of spacecraft fault tolerant control systems. In Sivasundaram, S., editor, *Nonlinear Problems in Aviation and Aerospace. Vol. 12: Advanced in Dynamics and Control*, pp. 309–331. CRC Press / Taylor & Francis.

Rodriguez-Donaire, S. et al. (2020). Earth observation technologies: low-end-market disruptive innovation. In *Satellites Missions and Technologies for Geosciences*, chapter 7, pp. 1–15. IntechOpen.

Schweighart, S. and Sedwick, R. (2002). High-fidelity linearized J2 model for satellite formation flight. *J. Guid. Control. Dyn.*, **25** (6), pp. 1073–1080.

Somov, Y., Butyrin, S., and Somov, S. (2021a). Autonomous attitude and orbit control of a space robot inspecting a geostationary satellite. *J. Phys. Conf. Ser.*, **1864** (012132), pp. 1–7.

Somov, Y., Butyrin, S., and Somov, S. (2021b). Dynamics of an autonomous spacecraft control system at initial transition to a tracking mode. *Cybernetics and Physics*, **10** (3), pp. 185–190.

Somov, Y., Butyrin, S., and Somov, S. (2023a). Control of a space robot approaching mini-satellites in low-orbit earth survey constellation. In *Proc. IEEE 2023 30th St. Petersburg Intern. Conf. on Integrated Navigation Systems*, pp. 1–4.

Somov, Y., Butyrin, S., and Somov, S. (2023b). Guidance, navigation and attitude control of mini-satellites in a low earth orbit constellation for areal survey. *Cybernetics and Physics*, **12** (2), pp. 145–151.

Sullivan, J., Grimberg, S., and D'Amico, S. (2017). Comprehensive survey and assessment of spacecraft relative motion dynamics models. *J. Guid. Control. Dyn.*, **40** (8), pp. 1837–1859.

Vallado, D. (2013). *Fundamentals of Astrodynamics and Applications*. Microcosm Press, Hawthorne. 1135 p.